Cell Reports, Volume *44*

Supplemental information

The STRIPAK complex is required for radial sorting and laminin receptor expression in Schwann cells

Michael R. Weaver, Dominika Shkoruta, Marta Pellegatta, Caterina Berti, Marilena Palmisano, Scott Ferguson, Edward Hurley, Julianne French, Shreya Patel, Sophie Belin, Matthias Selbach, Florian Ernst Paul, Fraser Sim, Yannick Poitelon, and M. Laura Feltri

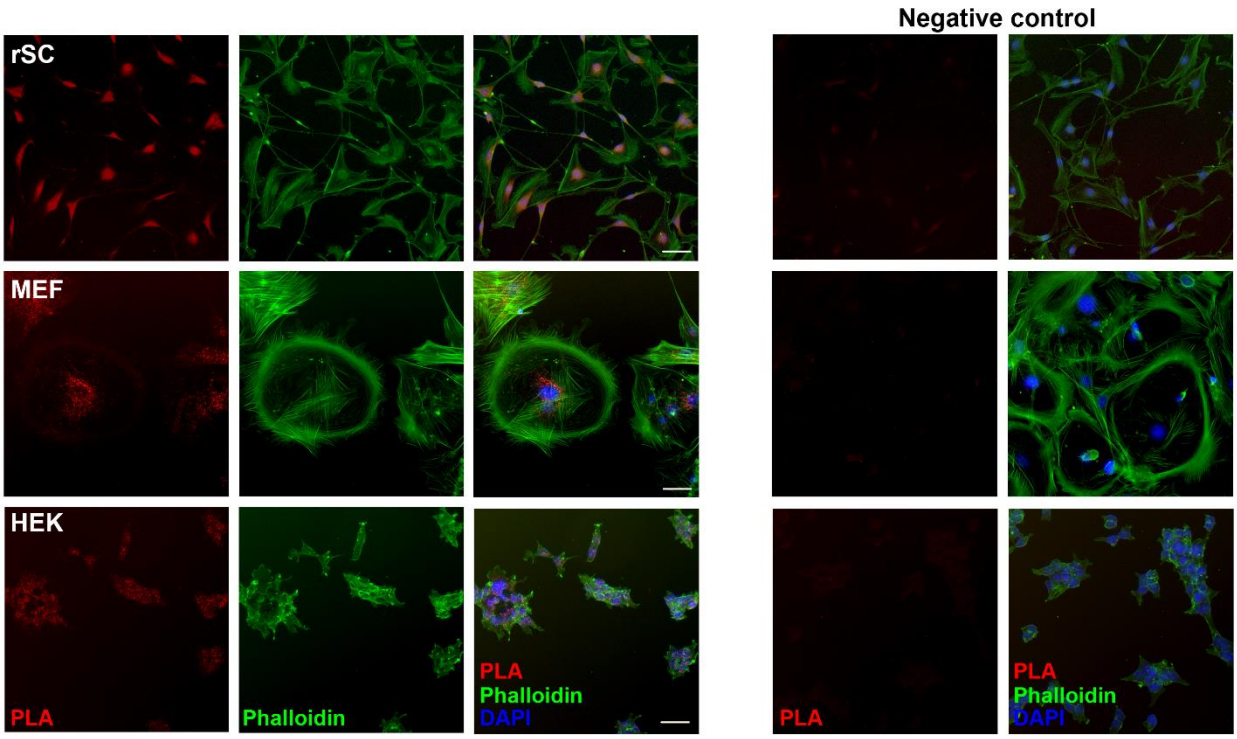

Supplementary Figure 1: STRN3 and Rac1 are in close proximity in vitro. Proximity ligation assay (PLA) technology permits the detection of protein-protein interactions in situ (< 40 nm). PLA analysis was performed in rat Schwann cells (rSC), mouse embryonic fibroblasts (MEF), and human embryonic kidney cells (HEK). The PLA analyses detected close localization (red dots) between STRN3 and Rac1 in the perinuclear region of rSC, MEF, and HEK. F-actin was stained with phalloidin (green) and nuclei were labeled with DAPI (blue). Negative controls lacking anti-STRN3 primary antibody did not produce PLA signals. Scale bar = 50 µm.

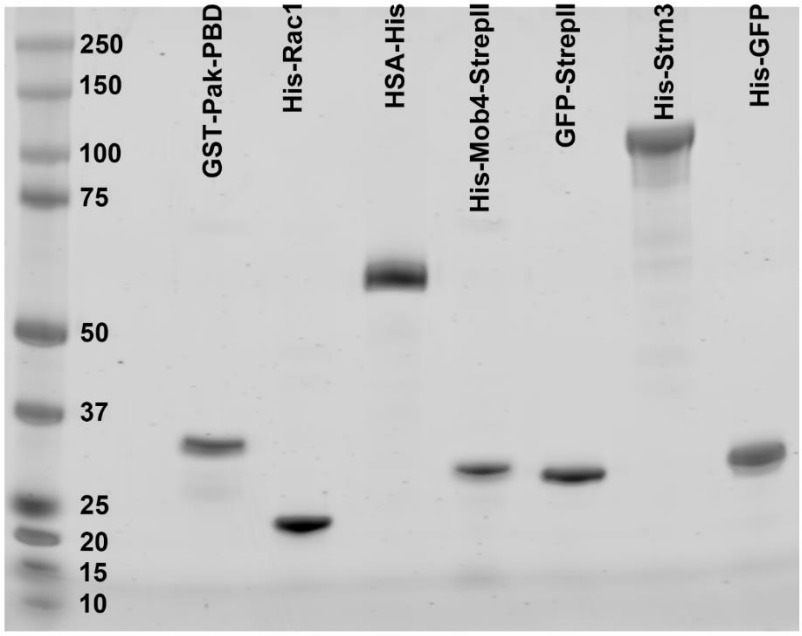

Supplementary Figure 2: Protein purification produced high yield of recombinant proteins. Gel electrophoresis for purified GST-PAK-PBD (Rac1/CDC42 binding domain (PDB) of p21 activated kinase 1 protein (PAK) labeled with a GST Tag; expected size 34kDa), His-Rac1 (Rac1 protein labeled with a His Tag, expected size 22 kDa), HSA-His (human serum albumin labeled with a His Tag; expected size 67 kDa), His-MOB4-StrepII (MOB4 protein labeled with a His Tag and a StrepII Tag, expected size 28 kDa), GFP-StrepII (green fluorescent protein labeled with a StrepII Tag, expected size 29 kDa), His-STRN3 (STRN3 protein labeled with a His Tag, expected size 95 kDa), His-GFP (green fluorescent protein labeled with a His Tag, expected size 33 kDa). Total proteins were stained with ReadyBlue.

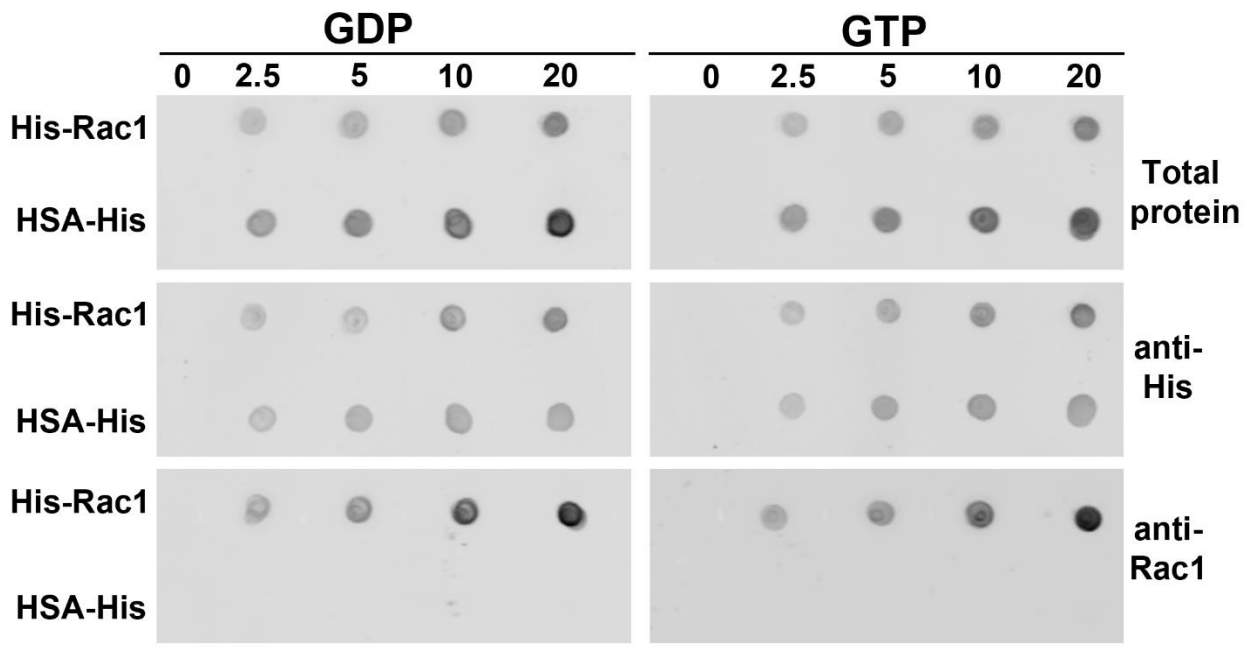

Supplementary Figure 3: Representative dot blot membranes showing bait dots prior to incubation with prey proteins. Bait proteins His-Rac1 (experimental) and HSA-His (negative control) were charged with either GDP or GTP and dotted in triplicate as a gradient (0, 2.5, 5, 10, and 20 pmoles). Membranes were separated by GDP/GTP charge state. Similar protein loading was observed for both GDP-charged and GTP-charged bait proteins by total protein staining and blotting with anti-His or anti-Rac1 antibodies. HSA-His has a higher molecular weight than His-Rac1, and therefore stains more intensely for total proteins when equal pmoles are loaded. Both bait proteins were labeled by anti-His blotting, but only His-Rac1 was labeled by anti-Rac1 blotting.

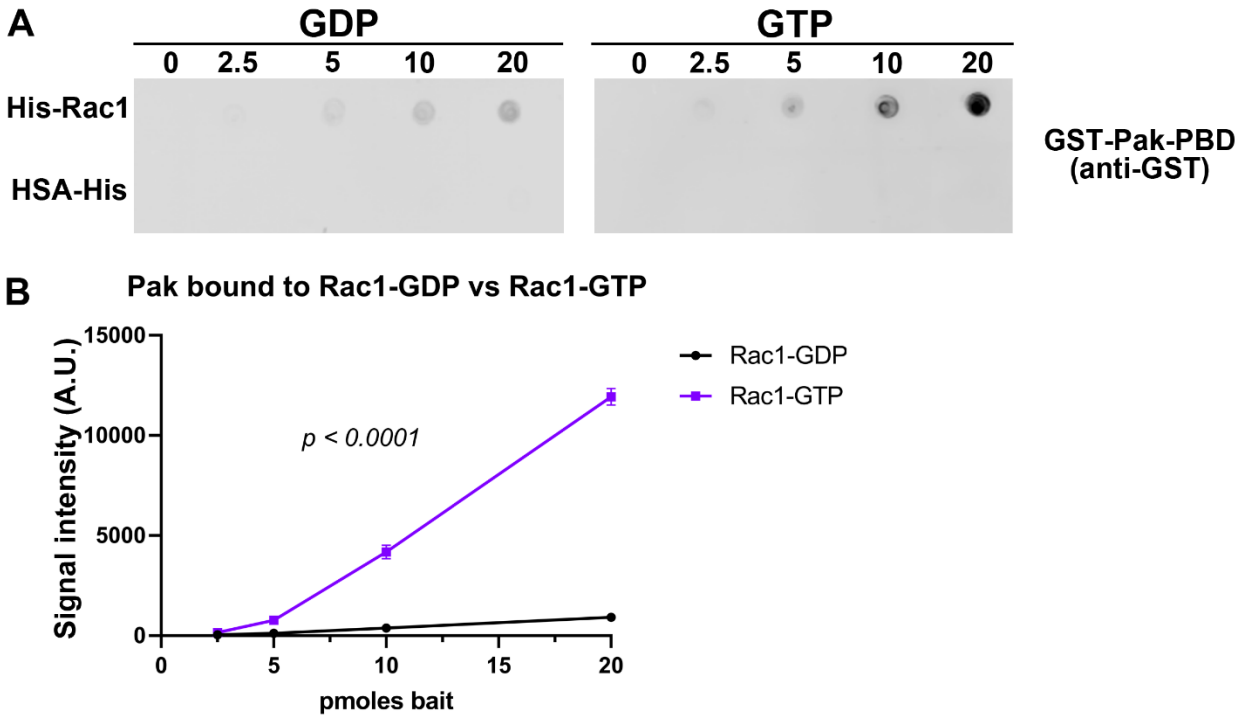

Supplementary Figure 4: His-Rac1 maintains GDP/GTP charge state during dot blot procedure. (**A**) Bait proteins His-Rac1 (experimental) and HSA-His (negative control) were charged with either GDP or GTP and dotted in triplicate as a gradient (0, 2.5, 5, 10, and 20 pmoles). Membranes were separated by GDP/GTP charge state. Dot blot membranes were incubated with prey protein GST-PAK-PBD and blotted for anti-GST. (**B**) Densitometry shows significantly more GST-PAK-PBD bound to His-Rac1-GTP as compared to His-Rac1-GDP. $N = 3$ individual dots per condition. Extra sum-of-squares F test. $F(2, 20) = 421.1$, $p < 0.0001$. Error bars indicate S.E.M. A.U.: Arbitrary Units.

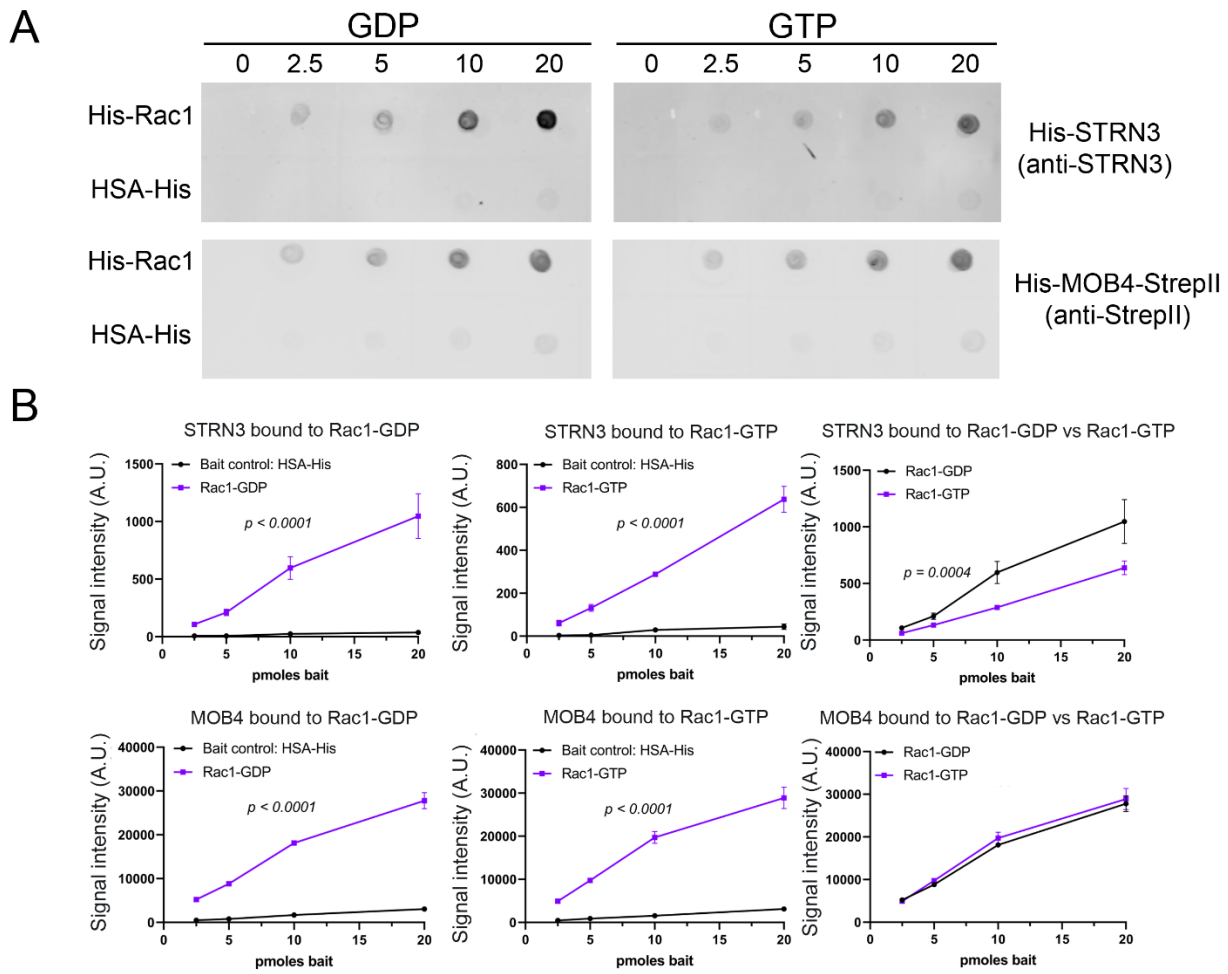

Supplementary Figure 5: STRN3 interacts directly with Rac1. (**A**) Bait proteins His-Rac1 (experimental) and HSA-His (negative control) were charged with either GDP or GTP and dotted in triplicate as a gradient (0, 2.5, 5, 10, and 20 pmoles). Membranes were separated by GDP/GTP charge state. Dot blot membranes were incubated with prey proteins His-STRN3 or His-MOB4-StrepII and blotted for anti-STRN3 or anti-StrepII, respectively. (**B**) Densitometry shows significantly more STRN3 bound to His-Rac1-GDP as compared to His-Rac1-GTP. In contrast, MOB4 bound to Rac1 independently of GDP/GTP charge state. *N* = 3 individual dots per condition. Extra sum-of-squares *F* test. A.U.: Arbitrary Units. Error bars indicate S.E.M. ** $p < 0.01$.

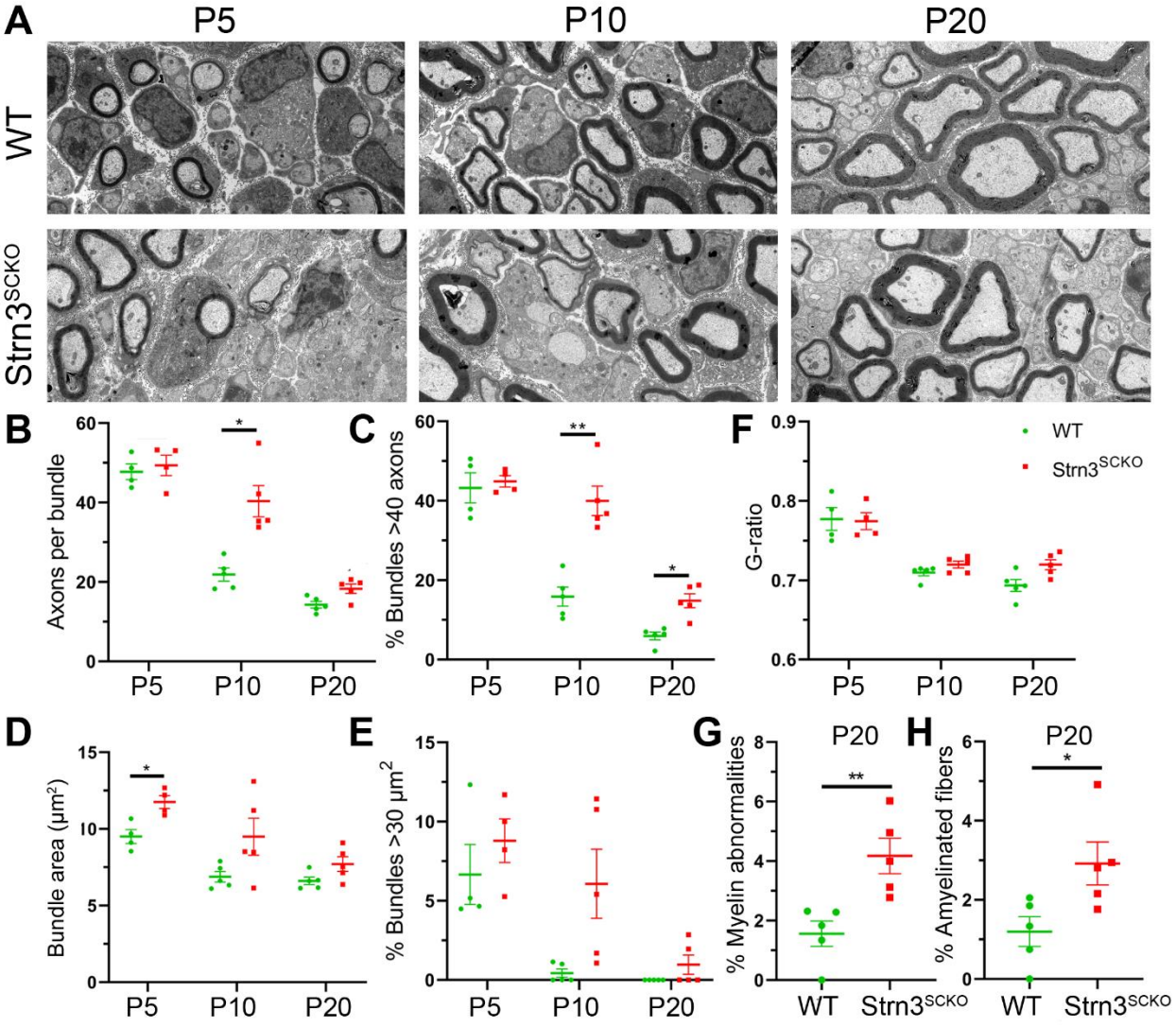

Supplementary Figure 6: Ablation of *Strn3* in SCs results in mild radial sorting and myelin abnormalities. (**A**) Representative electron microscopy images of WT and Strn3^{SCKO} sciatic nerves at P5, P10, and P20. Scale bar = 2µm. (**B**-**C**) Sciatic nerves of Strn3^{SCKO} mice have significantly more axons per unsorted, mixed-caliber axon bundle and significantly more bundles with many (>40) axons at P10. Two-way multiple comparisons ANOVA with Bonferroni post hoc test. Axons per bundle (F (1.743, 12.20) age = 137.3; $p < 0.0001$; F (1, 8) genotype = 11.11, $p = 0.0103$; $p_{P5} > 0.9999$, $p_{P10} = 0.0190$, $p_{P20} = 0.0751$). Bundles > 40 axons (F (1.299, 9.092) age = 95.32; $p < 0.0001$; F (1, 8) genotype = 24.09, $p = 0.0012$; $p_{P5} > 0.9999$, $p_{P10} = 0.0031$, $p_{P20} = 0.0122$). (**D**-**E**)

Sciatic nerves of Strn3^{SCKO} mice have significantly larger axonal bundles at P5. Two-way multiple comparisons ANOVA with Bonferroni post hoc test. Bundle area (F (1.475, 10.33) age = 19.01; p = 0.0006; F (1, 8) genotype = 7.872, p = 0.0230; p_{P5} = 0.0327, p_{P10} = 0.2837, p_{P20} = 0.2592). Bundles > 30 µm^2 (F (1.354, 14.89) age = 15.19; p = 0.0007; F (1, 22) genotype = 7.599, p = 0.0115; p_{P5} > 0.9999, p_{P10} = 0.1821, p_{P20} = 0.5626). (**F**) G-ratio (myelin thickness) is not significantly altered in sciatic nerves of Strn3^{SCKO} mice. Two-way multiple comparisons ANOVA with Bonferroni post hoc test. G-ratio (F (2, 11) age = 43.83; p < 0.0001; F (1, 11) genotype = 2.763, p = 0.1247; p_{P5} > 0.9999, p_{P10} > 0.9999, p_{P20} = 0.1170). (**G**) At P20, sciatic nerves of Strn3^{SCKO} mice have a significantly higher percentage of axons with myelin abnormalities, such as myelin infoldings, outfoldings, and decompaction. Unpaired two-tailed t-test (t = 3.568, df = 8, p = 0.0073). (**H**) At P20, sciatic nerves of Strn3^{SCKO} mice have a significantly higher percentage of sorted, amyelinated fibers. Unpaired two-tailed t-test (t = 2.605, df = 8, p = 0.0314). N = 4-5 samples per genotype. Error bars indicate S.E.M. (**B-F**) Two-way multiple comparisons ANOVA with Bonferroni post hoc test. *p < 0.05, ** p < 0.01.

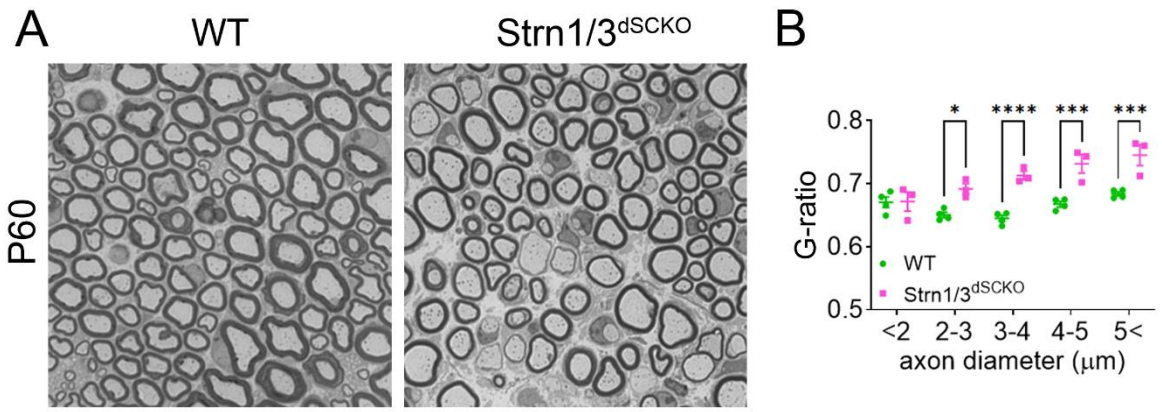

Supplementary Figure 7: *Strn1* and *Strn3* ablation in SCs results in reduced myelin thickness. (**A**) Representative semithin section images of WT and Strn1/3^{dSCKO} sciatic nerves at P60. Scale bar = 5μm. (**B**) G-ratio (myelin thickness) is significantly reduced in sciatic nerves of Strn1/3^{dSCKO} mice. Two-way multiple comparisons ANOVA with Bonferroni post hoc test. G-ratio (F (4, 25) axon diameter = 25.45; $p < 0.0001$; F (1, 25) genotype = 47.19, $p < 0.0001$; $p_{<2} > 0.9999$, $p_{2\text{-}3} > 0.0144$, $p_{3\text{-}4} < 0.0001$, $p_{4\text{-}5} > 0.0001$, $p_{5<} < 0.0002$). *$p < 0.05$, *** $p < 0.001$, **** $p < 0.0001$.

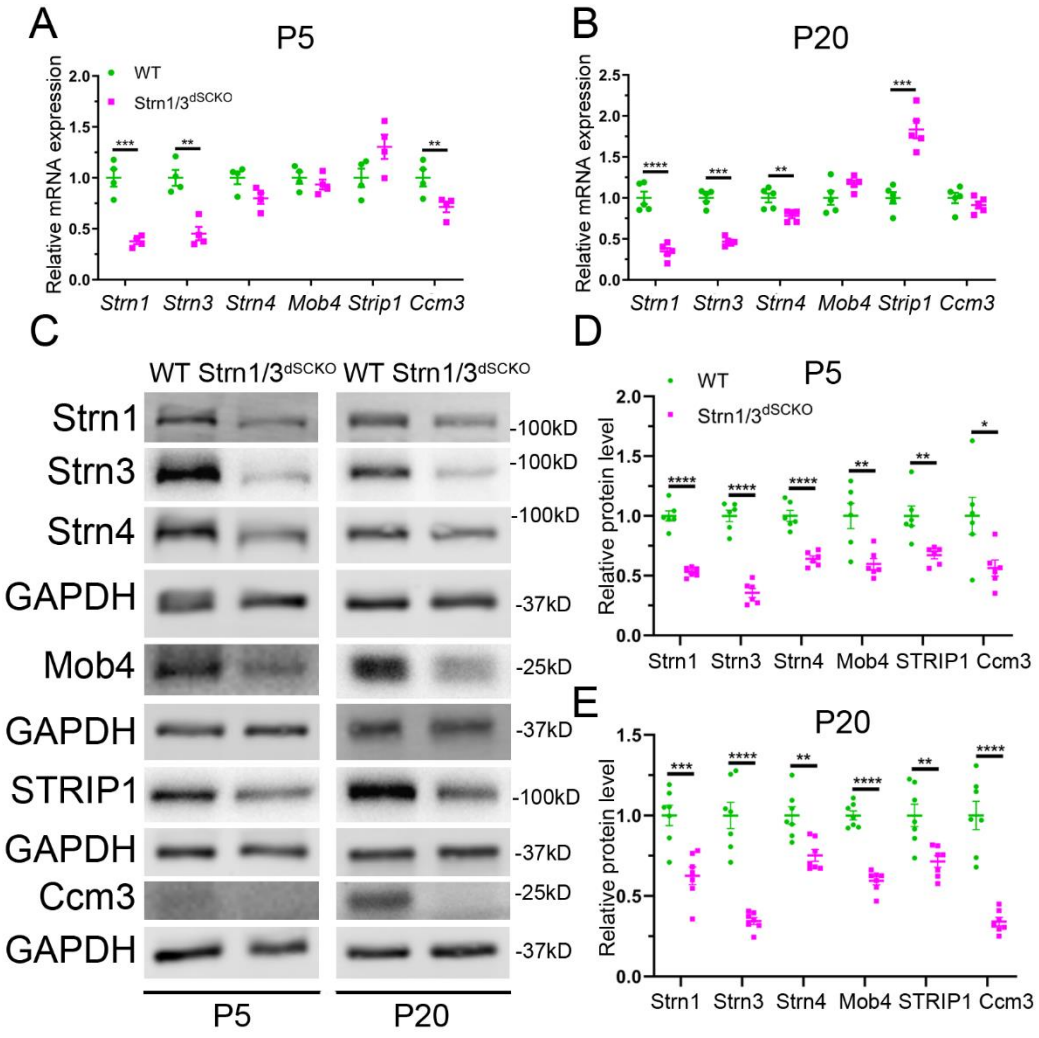

Supplementary Figure 8: *Strn1* and *Strn3* ablation in SCs results in reduced levels of STRIPAK proteins. (**A-B**) mRNA expression of several STRIPAK members from pooled sciatic nerves and brachial plexuses of WT and Strn1/3^{dSCKO} mice at P5 and P20. *Strn1* and *Strn3* mRNA levels are reduced at P5 and P20, *Ccm3* mRNA levels are reduced at P5, and *Strn4* mRNA levels are reduced at P20, and *Strip1* mRNA levels are increased at P20 in peripheral nerves of Strn1/3^{dSCKO} mice. *N* = 4-5 samples per genotype. P5 samples were pooled from 3-6 animals each. Unpaired two-tailed *t*-test. P5 [*Strn1* (t = 6.935, df = 6, p = 0.0004), *Strn3* (t = 5.385, df = 6, p = 0.0017), *Strn4* (t = 2.427, df = 6, p = 0.0514), *Mob4* (t = 0.8836, df = 6, p = 0.4109), *Strip1* (t = 2.032, df = 6, p = 0.0884), *Ccm3* (t = 2.906, df = 6, p = 0.0271)]. P20 [*Strn1* (t = 7.531, df = 8, p < 0.0001), *Strn3* (t = 10.48, df = 8, p < 0.0001), *Strn4* (t = 3.456, df = 8, p = 0.0086), *Mob4* (t =

0.1.858, df = 8, p = 0.1002), *Strip1* (t = 6.519, df = 8, p = 0.002), *Ccm3* (t = 1.140, df = 8, p = 0.2871)]. (**C**) Representative western blots of several STRIPAK proteins from pooled sciatic nerves and brachial plexuses of WT and Strn1/3^{dSCKO} mice at P5 and P20. (**D**-**E**) Densitometry analysis shows a reduction in STRN1, STRN3, STRN4, MOB4, STRIP1, and CCM3 protein levels in peripheral nerves of Strn1/3^{dSCKO} mice at P5 and P20. N = 6-7 samples per genotype. P5 samples were pooled from 3-6 animals each. Unpaired two-tailed t-test. P5 [STRN1 (t = 10.20, df = 10, p < 0.0001), STRN3 (t = 10.56, df = 10, p < 0.0001), STRN4 (t = 6.998, df = 10, p < 0.0001), MOB4 (t = 3.506, df = 10, p = 0.0057), STRIP1 (t = 3.718, df = 10, p = 0.0040), CCM3 (t = 2.585, df = 10, p = 0.0272)]. P20 [STRN1 (t = 4.497, df = 12, p = 0.0007), STRN3 (t = 7.770, df = 12, p < 0.0001), STRN4 (t = 3.842, df = 12, p = 0.0023), MOB4 (t = 10.84, df = 12, p < 0.0001), STRIP1 (t = 3.661, df = 12, p = 0.0033), CCM3 (t = 7.213, df = 12, p < 0.0001)]. Error bars indicate S.E.M. *p < 0.05, ** p < 0.01, *** p < 0.001, **** p < 0.0001.

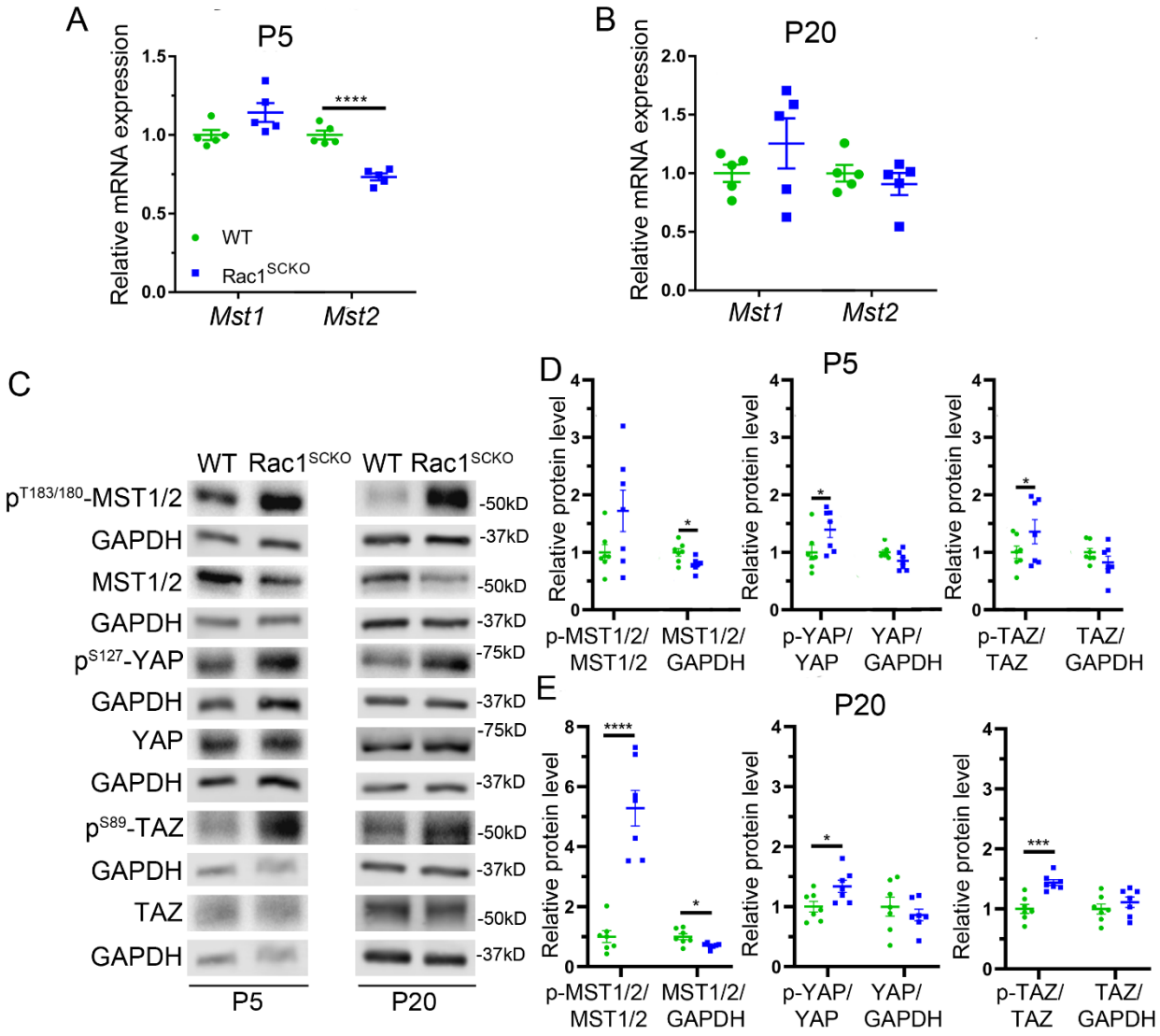

Supplementary Figure 9: *Rac1* ablation in SCs results in Hippo pathway dysregulation. (**A-B**) mRNA expression of *Mst1* and *Mst2* from pooled sciatic nerves and brachial plexuses of WT and Rac1^{SCKO} mice at P5 and P20. *Mst2* mRNA level is decreased at P5 in peripheral nerves of Rac1^{SCKO} mice. *N* = 5 samples per genotype. P5 samples were pooled from 3-6 animals each. Unpaired two-tailed *t*-test. P5 [*Mst1* (*t* = 2.105, df = 8, *p* = 0.0684), *Mst2* (*t* = 7.480, df = 8, *p* < 0.0001)]. P20 [*Mst1* (*t* = 1.123, df = 8, *p* = 0.2942), *Mst2* (*t* = 0.7793, df = 8, *p* = 0.4582)]. (**C**) Representative western blots of several Hippo pathways members from pooled sciatic nerves and brachial plexuses of WT and Rac1^{SCKO} mice at P5 and P20. (**D-E**) Densitometry analysis shows a reduction in MST1/2 total protein levels at P5 and P20, an increase in p-MST1/2 at P20, and an

increase in p-YAP and p-TAZ at P5 and P20 in peripheral nerves of $Rac1^{SCKO}$ mice. *N* = 6-7 samples per genotype. P5 samples were pooled from 3-6 animals each. Unpaired two-tailed *t*-test. P5 [p-MST1/2 ($t = 1.965$, df = 12, $p = 0.0730$), MST1/2 ($t = 2.750$, df = 12, $p = 0.0176$), p-YAP ($t = 2.998$, df = 12, $p = 0.0111$), YAP ($t = 2.059$, df = 12, $p = 0.0619$), p-TAZ ($t = 2.794$, df = 12, $p = 0.0162$), TAZ ($t = 1.334$, df = 12, $p = 0.2069$)]. P20 [p-MST1/2 ($t = 6.877$, df = 12, $p < 0.0001$), MST1/2 ($t = 2.908$, df = 12, $p = 0.0131$), p-YAP ($t = 2.512$, df = 12, $p = 0.0273$), YAP ($t = 0.7448$, df = 12, $p = 0.4707$), p-TAZ ($t = 4.867$, df = 12, $p = 0.0004$), TAZ ($t = 0.9376$, df = 12, $p = 0.3670$)]. Error bars indicate S.E.M. *$p < 0.05$, ** $p < 0.01$, *** $p < 0.001$, **** $p < 0.0001$.

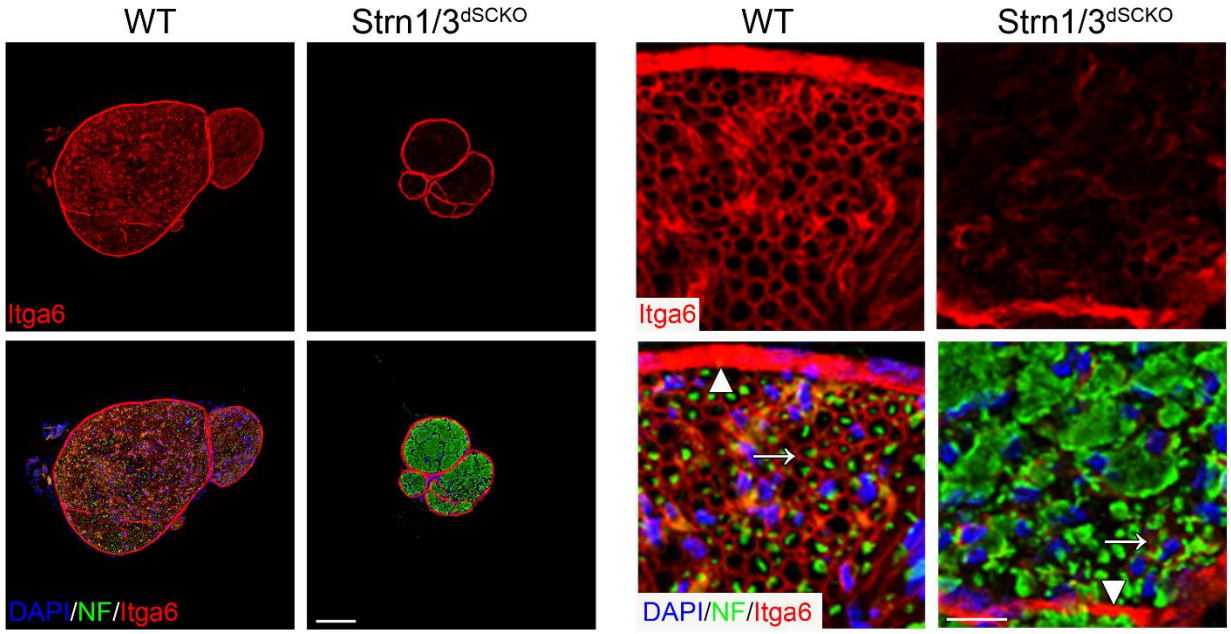

Supplementary Figure 10: *Strn1* and *Strn3* ablation in SCs results in reduced integrin α6 subunit expression. Sciatic nerve cross sections from WT and Strn1/3^{dSCKO} mice at P20 stained for integrin α6 subunit (Itga6, red). Axons are labeled by neurofascin (NF, green) and nuclei are labeled with DAPI (blue). White arrows indicate integrin α6 expression by SCs surrounding axons and white arrowheads indicate integrin α6 expression by perineurial cells in the perineurium. Integrin α6 appears drastically reduced in SCs, but not in the perineurium, in sciatic nerves of Strn1/3^{dSCKO} mice at P20. Scale bar = 100µm (left), 10µm (right).

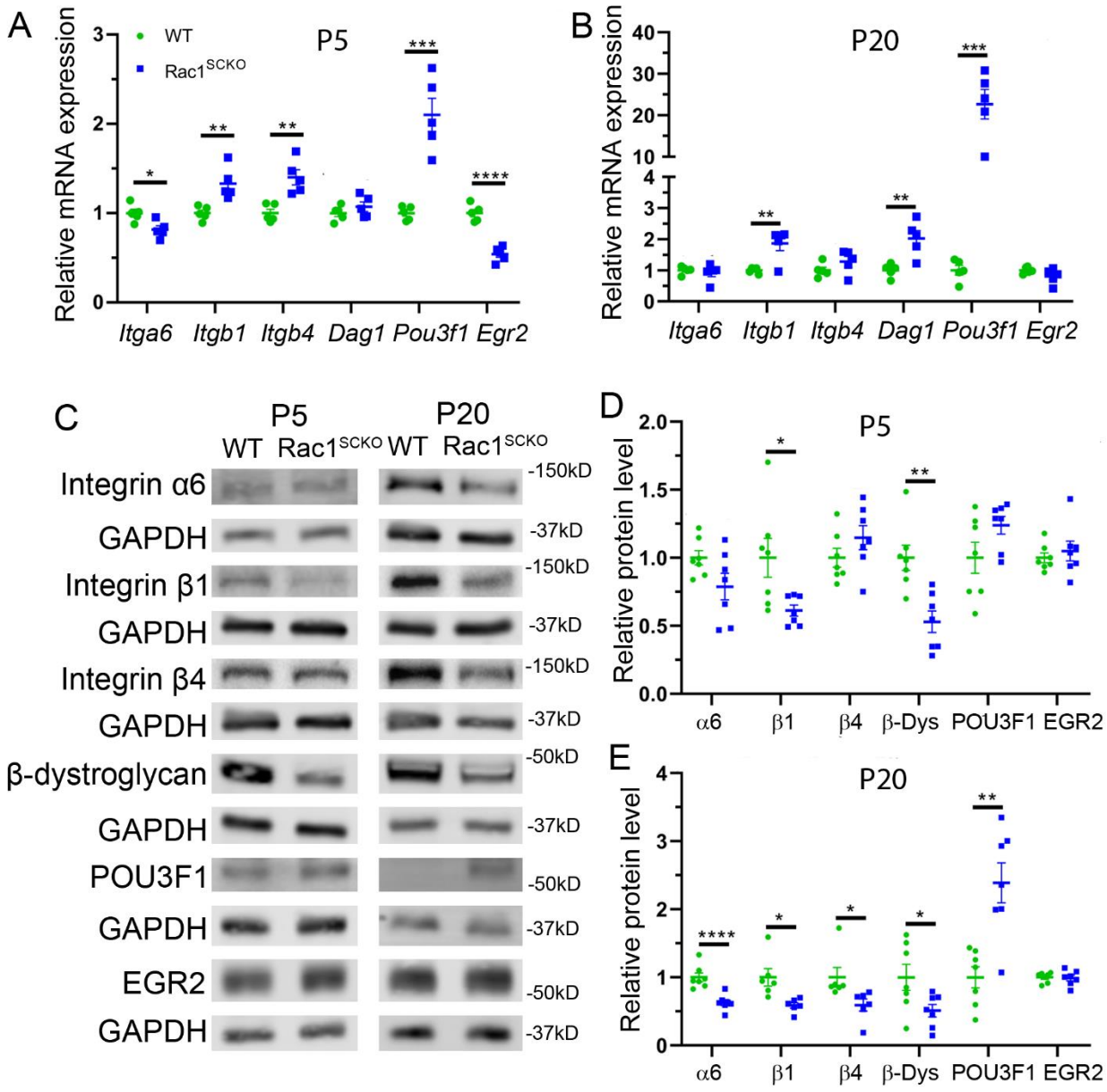

Supplementary Figure 11: *Rac1* ablation in SCs results in dysregulated mRNA and protein expression of laminin receptors and SC transcriptional regulators. (**A**-**B**) mRNA expression of several laminin receptors (encoding for integrin subunit α6 (*Itga6*), β1 (*Itgb1*), β4 (*Itgb4*), and β-dystroglycan (*Dag1*)) and SC development transcriptional regulators (*Pou3f1* and *Egr2*) from pooled sciatic nerves and brachial plexuses of WT and Rac1^{SCKO} mice at P5 and P20. *Itga6* and *Egr2* mRNA levels are decreased at P5, *Itgb1* and *Pou3f1* mRNA levels are increased at P5 and P20, *Itgb4* mRNA level is increased at

P5, and *Dag1* mRNA level is increased at P20 in peripheral nerves of Rac1^{SCKO} mice. *N* = 5 samples per genotype. P5 samples were pooled from 3-6 animals each. Unpaired two-tailed *t*-test. P5 [*Itga6* (t = 3.042, df = 8, p = 0.0160), *Itgb1* (t = 3.771, df = 8, p = 0.0055), *Itgb4* (t = 4.199, df = 8, p = 0.0030), *Dag1* (t = 1.086, df = 8, p = 0.3089), *Pou3f1* (t = 5.829, df = 8, p = 0.0004), *Egr2* (t = 8.147, df = 8, p < 0.0001)]. P20 [*Itga6* (t = 0.5845, df = 8, p = 0.5750), *Itgb1* (t = 3.717, df = 8, p = 0.0059), *Itgb4* (t = 1.418, df = 8, p = 0.1940), *Dag1* (t = 3.793, df = 8, p = 0.0053), *Pou3f1* (t = 6.063, df = 8, p = 0.0003), *Egr2* (t = 1.580, df = 8, p = 0.1529)]. (**C**) Representative western blots of several laminin receptors and SC development transcriptional regulators from pooled sciatic nerves and brachial plexuses of WT and Rac1^{SCKO} mice at P5 and P20. (**D**-**E**) Densitometry analysis shows a reduction in integrin β1 subunit and β-dystroglycan (β-Dys) at P5 and P20, integrin α6 and β4 subunits at P20, and an increase in POU3F1 at P20 in peripheral nerves of Rac1^{SCKO} mice. *N* = 6-7 samples per genotype. P5 samples were pooled from 3-6 animals each. Unpaired two-tailed *t*-test. P5 [integrin α6 (t = 0.2671, df = 12, p = 0.7939), integrin β1 (t = 2.619, df = 12, p = 0.0224), integrin β4 (t = 1.313, df = 12, p = 0.2139), β-dystroglycan (t = 4.697, df = 12, p = 0.0005), POU3F1 (t = 4.127, df = 12, p = 0.0014), EGR2 (t = 0.6095, df = 12, p = 0.5535)]. P20 [integrin α6 (t = 4.791, df = 12, p = 0.0004), integrin β1 (t = 3.086, df = 10, p = 0.0115), integrin β4 (t = 2.389, df = 10, p = 0.0380), β-dystroglycan (t = 2.304, df = 12, p = 0.0399), POU3F1 (t = 4.166, df = 12, p = 0.0013), EGR2 (t = 0.2044, df = 12, p = 0.8415)]. Error bars indicate S.E.M. *p < 0.05, ** p < 0.01, *** p < 0.001, **** p < 0.0001.

Primers	Sequences
MPZ-Cre A	CCACCACCTCTCCATTGCAC
MPZ-Cre AS2	GCTGGCCCAAATGTTGCTGG
MPZ-Cre 5MP2	TGTTGGCAACTTTGGATGTGT
MPZ-Cre P3P	TCAGCCAAGCCTTACCTTACT
Strn1 floxed forward	TGAATTATTGGAGTTTTGTTTCAGACC
Strn1 floxed reverse	GCACAGACAGACCTTCATGCTAACC
Strn3 floxed forward	ACCACAAAACAAGTGGTAGCTGAACC
Strn3 floxed reverse	TGAAGGTGGTAGGAATACAGAATAGCC
Strn4 floxed forward	CAGAGCAGCTGCTTGGCATAGAG
Strn4 floxed reverse	CACAACCGTGCACACTGGTGC
Rac1 floxed 1	ATTTTGTGCCAAGGACAGTGACAAGCT
Rac1 floxed 2	GAAGGAGAAGAAGCTGACTCCCATC
Rac1 floxed 3	CAGCCACAGGCAATGACAGATGTTC

Supplementary Table 1: Genotyping primer sequences

Primers	**Sequences / Taqman Probes**
Itga6 forward	CCTGAAAGAAAATACCAGACTCTCA
Itga6 reverse	GGAACGAAGAACGAGAGAGG
Itgb1 forward	CAACCACAACAGCTGCTTCTAA
Itgb1 reverse	TCAGC CCTCTTGAATTTTAATGT
Itgb4 forward	CTTGGTCGCCGTCTGGTA
Itgb4 reverse	TCGAAGGACACTACCCCACT
Dag1 forward	CTGCTGCTGCTCCCTTTC
Dag1 reverse	GCAGTGTTGAAAACCTTATCTTCC
Gapdh forward	CAACTCCCTCAAGATTGTCAGCAA
Gapdh reverse	GGCATGGACTGTGGTCATGA
Ccm3 (Taqman)	Mm00727342_s1
Egr2/Krox20 (Taqman)	Mm00456650_m1
Gapdh (Taqman)	Mm99999915_g1
Mst1 (Taqman)	Mm00451755_m1
Mst2 (Taqman)	Mm00490480_m1
Mob4 (Taqman)	Mm00481145_m1
Pou3f1/Oct6 (Taqman)	Mm00843534_s1
Strip1 (Taqman)	Mm00463714_m1
Strn1 (Taqman)	Mm00448910_m1
Strn3 (Taqman)	Mm00453492_g1
Strn4 (Taqman)	Mm00467125_m1
Taz (Taqman)	Mm01289583_m1
Yap (Taqman)	Mm01143263_m1

Supplementary Table 2: qPCR primer sequences and Taqman probes